High-spin ground states via electron delocalization in mixed-valence imidazolate-bridged divanadium complexes

Bettina Bechlars[1], Deanna M. D'Alessandro[1], David M. Jenkins[1], Anthony T. Iavarone[1], Starla D. Glover[2], Clifford P. Kubiak[2] and Jeffrey R. Long[1]*

The field of molecular magnetism has grown tremendously since the discovery of single-molecule magnets, but it remains centred around the superexchange mechanism. The possibility of instead using a double-exchange mechanism (based on electron delocalization rather than Heisenberg exchange through a non-magnetic bridge) presents a tantalizing prospect for synthesizing molecules with high-spin ground states that are well isolated in energy. We now demonstrate that magnetic double exchange can be sustained by simple imidazolate bridging ligands, known to be well suited for the construction of coordination clusters and solids. A series of mixed-valence molecules of the type $[(PY5Me_2)V^{II}(\mu-L_{br})V^{III}(PY5Me_2)]^{4+}$ were synthesized and their electron delocalization probed through cyclic voltammetry and spectroelectrochemistry. Magnetic susceptibility data reveal a well-isolated $S = 5/2$ ground state arising from double exchange for $[(PY5Me_2)_2V_2(\mu-5,6-dimethylbenzimidazolate)]^{4+}$. Combined modelling of the magnetic data and spectral analysis leads to an estimate of the double-exchange parameter of $B = 220$ cm^{-1} when vibronic coupling is taken into account.

Since the discovery of magnetic bistability in the molecular cluster $[Mn_{12}O_{12}(CH_3CO_2)_{16}(H_2O)_4]$, widespread research effort has been devoted to understanding the behaviour of such single-molecule magnets and to generating new clusters with higher blocking temperatures[1–4]. This effort is driven in part by the potential for applications of these molecules in information storage, quantum computing and spin-based molecular electronics[5–7]. It is interesting to note, however, that although the high-spin ground states for all single-molecule magnets discovered to date arise as a result of magnetic superexchange, most permanent magnets with high ordering temperatures are instead based on magnetism developed via itinerant electrons[8,9]. A key step in advancing molecular magnets towards technological viability may therefore involve the introduction of methods for establishing facile electron exchange within high-spin molecules. We envision a chemistry in which the tremendous strides recently made in the assembly of transition metal coordination clusters[10–14] are applied in creating mixed-valence species showing a stable high-spin ground state as a consequence of electron delocalization.

Mixed-valence complexes, as exemplified by the Creutz–Taube ion $[(NH_3)_5Ru(\mu-pyz)Ru(NH_3)_5]^{5+}$ (pyz = pyrazine; ref. 15), contain two or more metal ions in different formal oxidation states, and provide a powerful probe of intermetal electron transfer processes through the analysis of their intervalence charge transfer (IVCT) transitions[16–21]. Depending on the extent of electron delocalization, the systems may be classified as localized (Class I), weakly localized (Class II) or fully delocalized (Class III)[22]. In cases where the mixed-valence compounds contain metal ions with more than one unpaired electron, an intriguing phenomenon known as double exchange may be observed in the magnetic properties of the system due to the additional electronic contribution to the exchange coupling. This spin-dependent electron delocalization

phenomenon was first proposed by Zener in 1951 to explain the properties of mixed-valence manganites with perovskite structure[23]. The simultaneous occurrence of ferromagnetism and electronic conductivity at room temperature in these Class III compounds is understood by considering indirect coupling of the incomplete d-shells via the conduction electrons.

In a simplified picture, the conduction electrons are transferred between octahedral manganese centres, but retain their spin direction, thereby inducing a parallel alignment of the spins for all the incomplete d-shell electrons, as required to achieve the lowest energy configuration. Locally, two electrons are transferred simultaneously, one from a bridging O^{2-} anion to the Mn^{IV} centre and one from a Mn^{III} centre to the O^{2-} anion (Fig. 1). This concept of double exchange has been applied predominantly in the context of extended solids such as Heusler alloys[24], but in 1983 it was also introduced to molecular chemistry[25,26]. Despite a number
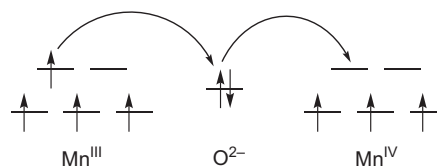
Figure 1 | Double-exchange mechanism in mixed-valence manganites. Two electrons are transferred simultaneously, one from a bridging O^{2-} anion to the Mn^{IV} centre and one from a Mn^{III} centre to the O^{2-} anion. The transferred electron that originates from Mn^{III} replaces that which was located on the O^{2-} anion, such that their spins are identical, in accordance with the Pauli principle. For the ground state, the spins of all unpaired electrons at the metal centres will then align parallel to the spin of the transferred electrons in accordance with Hund's rules.

[1]Department of Chemistry, University of California, Berkeley, California 94720-1460, USA, [2]Department of Chemistry and Biochemistry, University of California, San Diego, California 92093-0332, USA. *e-mail: jrlong@berkeley.edu
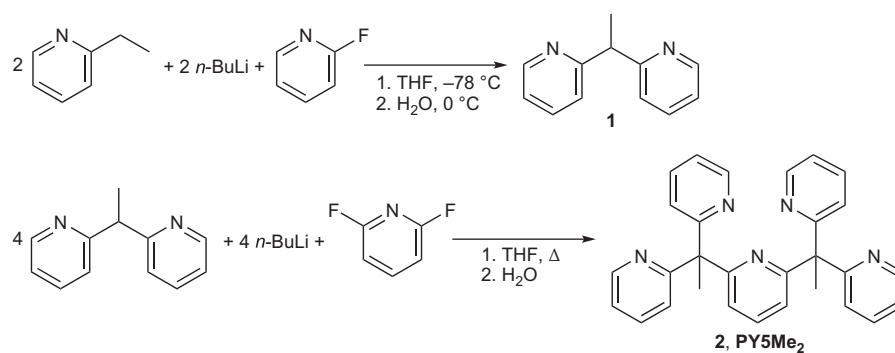
Figure 2 | Synthesis of the pentapyridine ligand PY5Me$_2$. The intermediate 1,1-*bis*(2-pyridyl)ethane (**1**) is obtained from the reaction of *n*-BuLi with 2-ethylpyridine and 2-fluoropyridine at −78 °C. PY5Me$_2$ (**2**) is subsequently obtained by lithiation of **1** with *n*-BuLi and reaction with 2,6-difluoropyridine. The ligand can be crystallized from dichloromethane and diethylether at −25 °C in 75% overall yield on a 25 g-scale.

of theoretical studies on this phenomenon[26–30], few experimental investigations have appeared[31–37]. By far the most thoroughly investigated system is [(Me$_3$tacn)Fe(μ-OH)$_3$Fe(Me$_3$tacn)]$^{2+}$ (Me$_3$tacn = N,N',N''-trimethyl-1,4,7-triazacyclononane)[34–37], a Class III mixed-valence compound in which electron delocalization between the two iron(II/III) centres leads to an $S = 9/2$ ground state that is well separated from its excited spin states, as observed from variable-temperature magnetic susceptibility (χ_M) data.

The isotropic Heisenberg Hamiltonian is typically used to determine the energies of the spin states in exchange-coupled systems in which the spin carriers are completely localized on the magnetic sites. In such cases, the paramagnetic metal sites are separated by one or more bridging ligands, and a superexchange coupling mechanism is operative, as quantified by the exchange coupling constant J (ref. 26). In an exchange-coupled dinuclear mixed-valence system, the double-exchange mechanism arises (in addition to Heisenberg exchange) due to the presence of an extra itinerant electron that aligns the localized magnetic moments[26–30]. This requires electron delocalization between the metal centres (a Class III mixed-valence system), which can be achieved by the incorporation of symmetric bridging ligands with frontier orbitals appropriate for facilitating electron transfer. Because the itinerant electron retains its spin during transfer between the metal centres, double exchange induces a parallel alignment of spins in the system, even when Heisenberg exchange favours antiferromagnetic coupling. This underscores the significance of making use of the double-exchange phenomenon to design molecules with high-spin ground states.

The work presented herein provides the first systematic examination of the ability of a simple directional bridging ligand, of the type readily used in constructing coordination clusters[10–13], to mediate double exchange through electron delocalization. Dinuclear complexes of the general formula [L$_{cap}$M(μ-L$_{br}$)ML$_{cap}$]$^{n+}$ (L$_{cap}$ = capping ligand, L$_{br}$ = symmetric bidentate bridging ligand, M = metal ion) are particularly suitable for this purpose, because electron transfer and magnetic exchange interactions occur between two metal centres through a single bridging ligand.

The pentadentate ligand 2,6-*bis*(1,1-*bis*(2-pyridyl)ethyl)pyridine (ref. 38; PY5Me$_2$) was chosen as a capping group, because it dictates a rigid octahedral coordination environment about the metal centre, while leaving one site open for the bridging ligand. In addition, PY5Me$_2$ is relatively easy to synthesize in large quantities, and can be expected to prevent the dinuclear complexes from engaging in intermolecular exchange interactions. Vanadium(II/III) was selected for the metal ion system owing to the diffuse $3d_\pi$ orbitals, which should have good overlap with the π-type orbitals for a conjugated bridging ligand. Here, the near half-filled t_{2g} orbital set presents a high-spin analogue of the well-studied ruthenium(II/III) system.

Finally, imidazolate was chosen as a compact, symmetric and conjugated bridging ligand, for which appendage of electron-donating or -withdrawing substituents enables manipulation of the character of the frontier orbitals. Accordingly, we present a thorough evaluation of selected dinuclear complexes of the type [(PY5Me$_2$)V^{II}(μ-L$_{br}$)V^{II}(PY5Me$_2$)]$^{3+}$, where L$_{br}$ is a bridging imidazolate (im$^-$) or benzimidazolate (bzim$^-$) ligand or one of the following symmetric derivatives: 2-methylimidazolate (2-mim$^-$), 2-chloroimidazolate (2-clim$^-$), 5,6-dimethylbenzimidazolate (5,6-dmbzim$^-$) or 4,5-diphenylimidazolate (4,5-dpim$^-$).

Results and discussion

Synthesis. As mentioned, PY5Me$_2$ was selected for use as a capping ligand in directing the formation of a bridged dinuclear complex, while shielding the complex from engaging in exchange interactions with neighbouring complexes. This semi-rigid pentapyridine ligand is structurally analogous to 2,6-(*bis*(*bis*-2-pyridyl)methoxymethane)pyridine (PY5), a ligand used previously in generating octahedral coordination complexes for a wide range of first-row transition metals[39,40].

A high-yielding and straightforward synthetic route to PY5Me$_2$ (**2**) was developed, as illustrated in Fig. 2 (ref. 41; note that PY5Me$_2$ was prepared in one other instance by a different route). Following a protocol similar to one previously used for the synthesis of 2,6-*bis*(*bis*(2-pyridyl)methyl)pyridine (PY5H$_2$; ref. 38), the ligand can readily be prepared on a multigram scale. In contrast to PY5H$_2$, the quaternary carbon that connects the pyridine rings in PY5Me$_2$ is not sensitive to the presence of base. Metallation of PY5Me$_2$ was accomplished by reaction with [V(MeCN)$_6$]$^{2+}$ in acetonitrile, leading to the isolation of [(PY5Me$_2$)V(MeCN)]I$_2$ (**3**) and [(PY5Me$_2$)V(MeCN)](PF$_6$)$_2$ (**4**).

The dinuclear complexes [(PY5Me$_2$)$_2$V$_2$(μ-L$_{br}$)](PF$_6$)$_3$ (L$_{br}$ = im$^-$ (**9**), 2-mim$^-$ (**10**), 4,5-dpim$^-$ (**12**), bzim$^-$ (**13**), 5,6-dmbzim$^-$ (**14**)) were prepared through the reaction of 1 equiv. of NaL$_{br}$ with 2 equiv. of **4** in acetonitrile. The compound [(PY5Me$_2$)$_2$V$_2$(μ-2-clim$^-$)](PF$_6$)$_3$ (**11**) was synthesized by the addition of 2-chloroimidazole and sodium methoxide to a solution of 2 equiv. of **4** in acetonitrile. As an alternative method, compounds **9**, **13** and **14** were also synthesized by reaction of the mononuclear complexes [(PY5Me$_2$)V(L$_{br}$)](PF$_6$) (L$_{br}$ = im$^-$ (**16**), bzim$^-$ (**17**), 5,6-dmbzim$^-$ (**18**)) with 1 equiv. of **4**. The foregoing direct method, however, was found to produce the desired dinuclear complexes in higher yields (55–92%).

Single crystals of **12**·MeCN and **14**·3.5MeCN·Et$_2$O suitable for X-ray analysis were obtained, and the representative molecular structure of [(PY5Me$_2$)$_2$V$_2$(μ-5,6-dmbzim)]$^{3+}$ is shown in Fig. 3. As expected, the acetonitrile molecule in **4** has been replaced by the imidazolate derivative, which links two [(PY5Me$_2$)V]$^{2+}$ units.
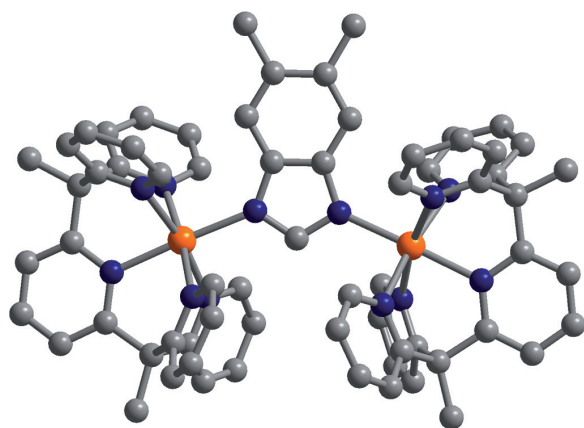
Figure 3 | Crystal structure of the dinuclear complex [(PY5Me$_2$)$_2$V$_2$(μ-5,6-dmbzim)]$^{3+}$ in 14·3.5MeCN·Et$_2$O. Orange, blue and grey spheres represent V, N and C atoms, respectively; H atoms are omitted for clarity. The imidazolate ligand provides a symmetric bridge between two V^{II} centres, each with an identical pseudooctahedral coordination sphere completed by the five pyridine rings of a PY5Me$_2$ ligand.

The V–N$_{im}$ distances are 2.188(4) and 2.195(4) Å in **12**·MeCN and 2.151(3) and 2.146(3) Å in **14**·3.5MeCN·Et$_2$O (details concerning some disorder with compound **14** can be found in the Supplementary Information). Owing to steric hindrance, the two phenyl rings of the 4,5-diphenylimidazolate ligand in **12**·MeCN are rotated relative to the plane of the five-membered imidazolate ring. It was not readily possible to obtain suitable single crystals for compounds **9**–**11** and **13**, and these complexes were instead characterized by mass spectrometry (Supplementary Fig. S5), with purity confirmed through elemental analysis.

The mixed-valence dinuclear complex [(PY5Me$_2$)$_2$V$_2$(μ-5,6-dmbzim)](PF$_6$)$_4$ (**15**) was obtained by adding 1.2 equiv. of [Cp$_2$Fe](PF$_6$) to an acetonitrile solution of **14**. To avoid subsequent reduction of the mixed-valence species, the reaction mixture was stirred for only two minutes before crystallization was induced by vapour diffusion of diethylether into the acetonitrile solution within 3 h. The molecular structure of **15** was confirmed by single-crystal X-ray diffraction. Here, the V–N$_{im}$ distances for the two vanadium sites differ more substantially, with V1–N$_{im}$ = 2.015(2) Å and V2–N$_{im}$ = 2.168(2) Å, suggesting a valence-localized (Class II) electronic structure in the solid state at 151 K.

Electrochemistry. The electrochemical properties of **9**–**14** were assessed using cyclic voltammetry. All six compounds show two reversible one-electron redox waves corresponding to successive oxidation of each V^{II} ion to V^{III} at different potentials (Fig. 4a). The separation between the two V$^{II/III}$ redox potentials provides evidence for electronic communication between the two metal ions. The peak positions $E_{1/2}(4 + /5 +)$ and $E_{1/2}(3 + /4 +)$ and peak separation $\Delta E_{1/2} = E_{1/2}(4 + /5 +) - E_{1/2}(3 + /4 +)$, determined in different electrolyte media, were used to calculate the comproportionation constants, $K_c = 10^{16.9\Delta E_{1/2}}$, for the reaction [(PY5Me$_2$)$_2$V$_2$(μ-L$_{br}$)]$^{3+}$ + [(PY5Me$_2$)$_2$V$_2$(μ-L$_{br}$)]$^{5+}$ ⇌ [(PY5Me$_2$)$_2$V$_2$(μ-L$_{br}$)]$^{4+}$ (Supplementary Table S1).

The K_c values determined from measurements in a 0.1 M solution of n-Bu$_4$N(PF$_6$) in benzonitrile were found to follow the trend **14** > **13** > **9** ≈ **10** > **11** > **12**, and range from 9.0×10^3 for **12** to 1.8×10^7 for **14**. Thus, by this measure, the degree of electronic communication between [(PY5Me$_2$)V]$^{n+}$ units follows the bridging ligand trend 5,6-dmbzim$^-$ > bzim$^-$ > im$^-$ ≈ 2-mim$^-$ > 2-clim$^-$ > 4,5-dpim$^-$.

Although the comparison of $\Delta E_{1/2}$ and K_c values determined from electrochemical data has been widely used for the assessment
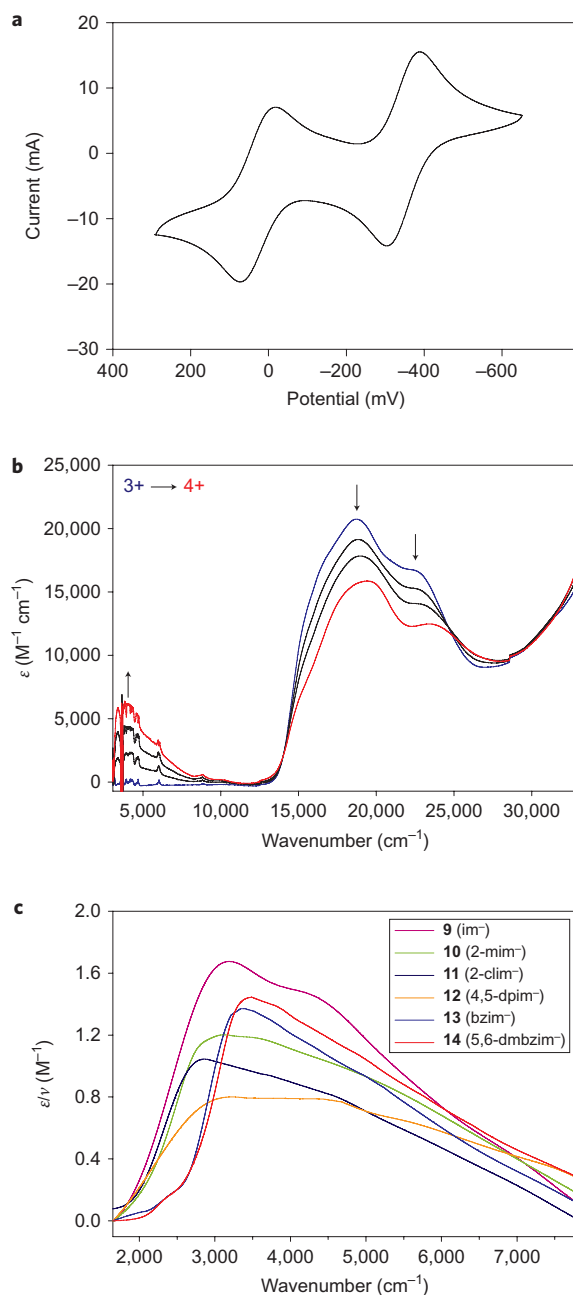
Figure 4 | Electrochemical and spectroscopic characterization of the imidazolate-bridged divanadium complexes. a, Cyclic voltammogram for the [(PY5Me$_2$)$_2$V$_2$(μ-5,6-dmbzim)]$^{3+}$ complex of **14** collected in a 0.1 M solution of n-Bu$_4$N(PF$_6$) in acetonitrile, with potentials referenced to the [Cp$_2$Fe]$^{0/1+}$ couple. Two reversible one-electron oxidation processes occur, centred at $E_{1/2}(3 + /4 +) = -387$ mV and $E_{1/2}(4 + /5 +) = +24$ mV, corresponding to succesive oxidations of the two V^{II} centres. A comproportionation constant of $K_c = 2.3 \times 10^6$ was obtained from the peak separation of $\Delta E_{1/2} = 376$ mV. **b**, Spectral progression accompanying the one-electron oxidation of compound **14**. The spectra were recorded in a 0.1 M solution of n-Bu$_4$N(B(C$_6$F$_5$)$_4$) in 1,2-difluorobenzene at increasing potentials ranging from +0.080 to +1.300 V versus [Cp$_2$Fe]$^{0/1+}$. As the intensity of the MLCT bands decrease, an IVCT band for the mixed-valence species appears in the NIR with increasing intensity. **c**, Overlay of the IVCT bands for the mixed-valence dinuclear complexes generated upon one-electron oxidation of compounds **9**–**14** in a 0.1 M solution of n-Bu$_4$N(PF$_6$) in benzonitrile. Note that all of the bands are asymmetrically shaped and narrower on the lower-energy side, a situation that is most pronounced for **13** and **14**.

of the extent of coupling in mixed-valence complexes[18,20,21], previous reports have emphasized the need for caution in the interpretation of electrochemical results, due to the significant dependence of redox potentials on the identity of the solvent and anions in the electrolyte medium[42]. Spectral measurements of the intervalence charge transfer (IVCT) transitions, as detailed below, serve as a more accurate probe of electron delocalization. In particular, the extent of delocalization can be extracted by analysing the IVCT band shape based on a theory derived by Hush and Marcus[16,20]. Supplementary Fig. S7 illustrates the differences in the band shape that can be expected for mixed-valence complexes with localized and delocalized classifications.

Spectroelectrochemistry. Changes in the UV/Vis/NIR (near-infrared) absorption spectrum during electrochemical oxidation of the 5,6-dmbzim⁻-bridged complex of **14** were measured at potentials ranging from +0.080 to +1.300 V versus $[Cp_2Fe]^{0/1+}$ using an optically semi-transparent thin-layer electrosynthetic cell. As shown in Fig. 4b, the initial spectrum of the divanadium(II) complex features a band with a maximum at 18,740 cm^{-1} and a shoulder at 22,090 cm^{-1}, which are assigned as metal-to-ligand charge transfer (MLCT) transitions.

The spectral progression accompanying the one-electron oxidation to afford the mixed-valence vanadium(II)–vanadium(III) species reveals stable isosbestic points. The MLCT absorption bands steadily decrease in intensity during the process, with the appearance of a new band in the NIR region (4,000–8,000 cm^{-1}). The intensity of this new band was seen to increase until it reached a maximum, and then decrease as the potential was held at a value beyond that required for generation of the two-electron oxidized species (Supplementary Fig. S8). On this basis, the band is assigned as an IVCT transition. The starting complex was regenerated in greater than 80% yield following the one-electron oxidation process. In addition, the mononuclear complex $[(PY5Me_2)V(5,6\text{-dmbzim})]^+$ in **18** and its one-electron oxidized analogue do not exhibit an absorption band in the NIR region of their electronic absorption spectra. This observation lends additional support to the assignment of an IVCT band for the dinuclear mixed-valence complex.

Owing to complications from overlapping solvent overtones and cut-off of the band at the limit of the NIR detector, FT-IR spectroelectrochemistry[43] in the region 1,500−8,000 cm^{-1} was used to examine the IVCT bands for the full series of mixed-valence dinuclear complexes. An overlay of the IVCT bands observed upon electrochemical oxidation of compounds **9–14** is shown in Fig. 4c, and the results of the band maxima (ν_{max}), molar absorption coefficients (ε_{max}) and bandwidths ($\Delta\nu_{1/2}$) are summarized in Supplementary Table S2. For all complexes, the IVCT bands are asymmetrically shaped and narrower on the lower energy side. A moment analysis of the bands was performed and the electronic coupling parameters H_{AB} were determined, as described in the Supplementary Information.

By comparison with the theoretical bandwidths ($\Delta\nu^{\circ}_{1/2} = (2,310(\nu_{max}))^{1/2}$ at 298 K) estimated on the basis of the classical two-state theory[16] $\Delta\nu_{1/2} < \Delta\nu^{\circ}_{1/2}$ for the mixed-valence forms of **13** and **14**, whereas $\Delta\nu_{1/2} > \Delta\nu^{\circ}_{1/2}$ for the mixed-valence forms of **9–12**. The results suggest that a localized description (Class II) is appropriate for the latter, whereas the one-electron oxidized forms of **13** and **14** exhibit relatively greater electronic delocalization (Class II–III)[19]. It should be noted, however, that the presence of vibronic coupling or multiple underlying IVCT components will broaden the IVCT band manifold.

From the moment analysis of the bands, the general trend is a decrease in the extent of delocalization in the series **14** (5,6-dmbzim⁻) ≈ **13** (bzim⁻) > **9** (im⁻) ≈ **10** (2-mim⁻) > **11** (2-clim⁻) ≈ **12** (4,5-dpim⁻). This result is consistent with the expectation that electron-withdrawing chloro and phenyl substituents on the
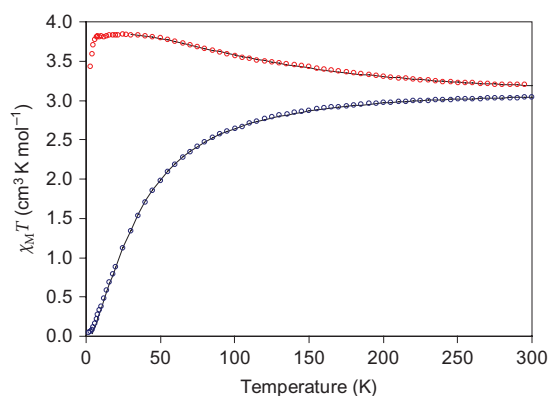
Figure 5 | Variable-temperature magnetic susceptibility data. Data for **14** (blue circles) and **15** (red circles) were collected in an applied field of 1 T. The black lines represent the best fit for each data set. With decreasing temperature, $\chi_M T$ drops steadily for the V^{II}-V^{II} complex in **14**, indicating antiferromagnetic coupling, but rises for the V^{II}-V^{III} complex in **15**, indicating a high-spin ground state arising from double exchange. The data for **14** were fit based on isotropic Heisenberg coupling to give $J = -6.0$ cm^{-1} and $g = 1.92$, while the data for **15** could be fit by including a double-exchange parameter of $B = 122$ cm^{-1}, together with $J = -4.4$ cm^{-1} and $g = 1.87$.

imidazolate bridging ligand reduce the electronic coupling between the metal centres, whereas electron-donating methyl substituents on the benzimidazolate or imidazolate bridging ligands lead to relatively stronger coupling. The trend is also consistent with that observed from cyclic voltammetry experiments.

The theoretical analysis of the IVCT data for the borderline localized-to-delocalized benzimidazolate-bridged systems is challenging, because the application of classical models[16,18] is strictly invalid due to failure of the Born–Oppenheimer approximation upon which they are based. Although the treatment of the full vibronic coupling problem is central to the quantitative analysis of these systems, the application of such methods is beyond the scope of the present work.

Magnetism and double exchange. The results of variable-temperature magnetic susceptibility measurements for compounds **9–13** and **14** are shown in Supplementary Fig. S9 and Fig. 5, respectively. All six compounds contain dinuclear complexes with the vanadium ions in the +II oxidation state. At room temperature, the observed $\chi_M T$ values for **9–14** fall in the range 3.04–3.77 cm^3 K mol^{-1}, close to the value of 3.75 cm^3 K mol^{-1} expected for two non-interacting V^{II} ($S = 3/2$) centres if the spectroscopic splitting factor, g, is 2.00. The gradual drop in $\chi_M T$ with decreasing temperature is indicative of weak antiferromagnetic exchange coupling due to superexchange between the two metal centres via the bridging ligand. Fits to the data sets using the Bleaney–Bowers equation for magnetic susceptibility enabled extraction of the coupling constants, J, which lie in the range –2.2 to –6.0 cm^{-1} (see Supplementary Table S3)[44,45]. Note that the strength of the coupling follows the trend **14** (5,6-dmbzim⁻) > **13** (bzim⁻) > **9** (im⁻) > **10** (2-mim⁻) > **11** (2-clim⁻) > **12** (4,5-dpim⁻), which is the same ordering observed for the extent of electron delocalization in the one–electron oxidized complexes based upon IVCT data.

Although the X-ray structural data for the mixed-valence compound **15** are consistent with the presence of localized valences, the results from variable-temperature magnetic susceptibility measurements indicate that the metal centres are indeed electronically coupled and show a double-exchange interaction (see Fig. 5). The $\chi_M T$ value of 3.19 cm^3 K mol^{-1} at 300 K is slightly above the value of 2.875 cm^3 K mol^{-1} expected for one V^{II} ($S = 3/2$) centre and

365
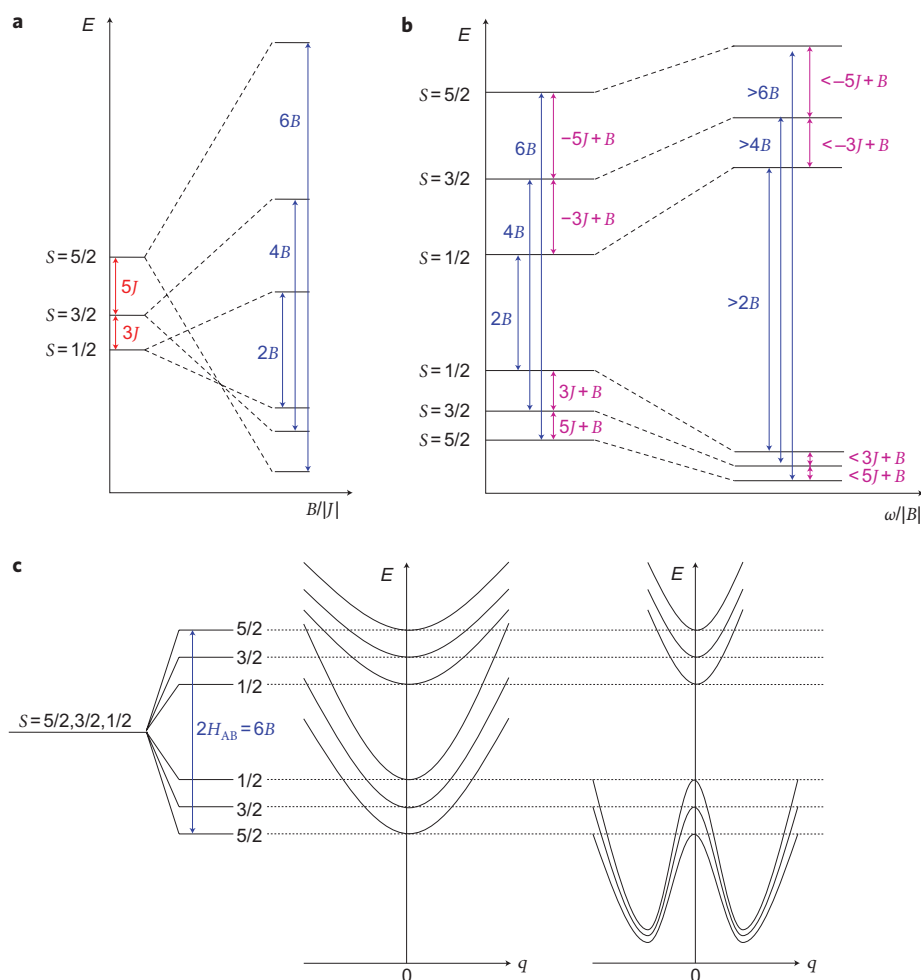
Figure 6 | Spin-state energy diagrams and adiabatic potentials under the influence of vibronic coupling. Plots are for a mixed-valence dinuclear complex containing antiferromagnetically coupled metal centres with $S_A = 3/2$ and $S_B = 1$. **a**, Effect of the double-exchange parameter B assuming complete electron delocalization. Note that if $B/|J|$ is sufficiently large, the order of spin-state energies is reversed. **b**, Perturbation of the energy levels due to vibronic coupling, in which the intermetal electron transfer couples to a vibrational mode of frequency ω. The vibronic coupling leads to an increased energy difference between symmetric and antisymmetric spin states and a decreased energy difference between the spin states of the same symmetry. **c**, Adiabatic potentials of the spin-state energies for a fully delocalized symmetrical dinuclear complex without (left) and with (right) vibronic coupling. In the absence of vibronic coupling only one minimum at $q = 0$ exists, whereas with vibronic coupling two minima are expected.

one V^{III} ($S = 1$) centre with $g = 2.00$ and no exchange interaction. In this case, rather than dropping with decreasing temperature, as would be in accord with the expected antiferromagnetic interaction arising from superexchange, $\chi_M T$ is seen to rise steadily, reaching a maximum of 3.83 cm^3 K mol^{-1} at 20 K.

This progression indicates the parallel alignment of the vanadium spins to give an $S = 5/2$ ground state, as could only arise from double exchange. This ground state was confirmed by fitting the data obtained from variable-field magnetization measurements at different temperatures to the Brillouin function for an $S = 5/2$ state (Supplementary Fig. S10). Note that the small downturn in $\chi_M T$ observed below 20 K is also consistent with the expected Zeeman contribution for the $S = 5/2$ ground state in an applied field of 1 T. Thus, although the complete delocalization associated with Class III mixed valence represents the most desirable situation for achieving double exchange, the results for [(PY5Me$_2$)$_2$V$_2$(μ-5,6-dmbzim)]$^{4+}$ provide an important initial demonstration that double exchange can also arise in a Class II–III molecule.

The isotropic Heisenberg Hamiltonian that is used to determine the energies of the spin states in an exchange-coupled dinuclear complex is not valid for a mixed-valence dinuclear complex with

additional intermetal electron transfer. For a symmetrical mixed-valence species, the electron can be located on either metal site with an equal probability. Therefore, Heisenberg exchange in such molecules leads to the occurrence of doubly degenerate spin states. Orbital interactions between the two metal sites will lift this degeneracy and lead to a splitting of the spin state energy levels into symmetric ($+$) and antisymmetric ($-$) states[28]. The spin state energies for a symmetrical dinuclear complex with intermetal electron exchange are then given as $E_\pm = -JS(S + 1) \pm B(S + 1/2)$, where B is the double-exchange parameter.

If we assume complete electron delocalization, the spin state energy diagram of **15** can be represented as shown in Fig. 6a. Note that when $B/|J|$ becomes sufficiently large, the splitting leads to a reverse ordering of the spin state energies ($S = 5/2 < S = 3/2 < S = 1/2$) compared with the solely exchange-coupled dinuclear complex ($S = 1/2 < S = 3/2 < S = 5/2$). This gives rise to the $S = 5/2$ ground state observed for compound **15**. Indeed, the variable-temperature magnetic susceptibility data for **15** could be fit as described in the Supplementary Information to obtain $J = -4.4$ cm^{-1}, $B = 122$ cm^{-1} and $g = 1.87$. These values indicate a weak antiferromagnetic Heisenberg exchange interaction, as expected based on orbital considerations and the

results observed for **14**, which is overwhelmed by the parallel spin alignment imposed by the double-exchange phenomenon. Importantly, this situation gives rise to a high-spin ground state that is well isolated in energy, with the $S = 5/2$ ground state lying 100 cm^{-1} below the $S = 3/2$ excited state.

The double-exchange parameter can also be extracted from the IVCT band of the mixed-valence compound. Assuming that the 'extra' electron in **15** is fully delocalized between the two vanadium centres, the energy of the most intense IVCT transition can be equated with the symmetric to antisymmetric spin state transition of a molecule in the ground state. As shown in Fig. 6a, this corresponds to $\Delta E(S = 5/2) = E_+(S = 5/2) - E_-(S = 5/2) = 6B$. The first moments of the IVCT bands for **15** are $M_1 = 4{,}190$ cm^{-1} (solid-state spectrum) and 4,580 cm^{-1} (in a 0.1 M solution of n-Bu$_4$N(PF$_6$) in benzonitrile), from which B values of 698 and 763 cm^{-1}, respectively, are obtained. Thus, the electron exchange parameter $B = 122$ cm^{-1}, extracted from the magnetic susceptibility measurements, is significantly smaller than the values resulting from the optical measurements using this fully delocalized model.

To understand the source of the discrepancy, the influence of vibronic coupling must be considered[28–30,46]. In a symmetric mixed-valence dinuclear complex, the exchange of the extra electron between the two metal centres leads to a deformation in their coordination spheres. The PKS vibronic coupling theory describes the coupling of the electron motion with the fully symmetric vibrational modes (breathing modes), which results in a localizing effect on the electron. The energy for the resulting spin states can then be calculated as follows:[28,46]

$$E_\pm(S) = -J_0 S(S+1) + \frac{\omega x_-^2}{2} \pm \left[B^2 (S + 1/2)^2 + \frac{\omega^2 x_-^2}{2} \right]^{1/2} \quad (1)$$

where $x_- (= q_-/(\lambda/k))$ is the antisymmetric reduced normal coordinate for a two-site one-electron problem, q the collective coordinate referring to in-phase $(q_+ = (1/(\sqrt{2})(q_A + q_B))$ and out-of-phase $(q_- = (1/\sqrt{2})(q_A - q_B))$ vibrations, $\omega (= \lambda^2/k)$ the vibrational frequency, k the force constant, λ the vibronic coupling parameter, and $B = H_{AB}/(S_0 + 1/2)$ the double-exchange parameter (with H_{AB} = electronic coupling parameter, S_0 = core spin).

Whereas the adiabatic potentials of the spin-state energies for a fully delocalized symmetrical dinuclear complex without vibronic coupling exhibit only one minimum at $q = 0$, two minima are observed when vibronic coupling is involved, as depicted in Fig. 6c. The energy diagram for the vibrational ground states then changes, as for example shown in Fig. 6b. If vibronic coupling dominates over double exchange (when $B(S + 1/2) < \omega/2$), the order of the lower-lying spin state energies is reversed and a low-spin ground state arises from Heisenberg exchange. On the other hand, if double exchange dominates over vibronic coupling (when $B(S + 1/2) > \omega/2$), the energy differences between the spin states will still change, but the order for the lower-lying states will be consistent with Fig. 6b. The energy difference between the E_- levels, and the energy difference between the E_+ levels will decrease compared to the fully delocalized system, whereas the energy differences between the symmetric and antisymmetric spin states of the same spin will increase. Thus, the most intense IVCT transition will be greater than $6B$. This reasoning may explain why the values for the double-exchange parameter extracted from optical measurements are larger than the value of 122 cm^{-1} extracted from the magnetic susceptibility data. In the latter case, we need only consider the low-lying energy states, E_-, because the high-lying energy states, E_+, will not be significantly populated in the temperature range evaluated. The smaller energy difference between the E_- levels leads to an underestimation of the B value

when the fit is based on a fully delocalized model. The true B value for compound **15** should therefore lie somewhere between 122 and 698 cm^{-1}.

Based on the PKS model, Girerd and colleagues suggested that the energy of the optical transition is independent of S ($E_{op} = \omega$), and that a Heisenberg Hamiltonian with the new coupling parameter $J_{eff} = J_0 + 2B^2/\omega$ is valid to calculate the energies of the spin states, if it can be assumed that $B(S + 1/2) < \omega/2$ for all $E_-(S)$ (ref. 28). Applying this formula to the optical data for **15**, we can extract ω from the IVCT band because $E_{op} = \nu_{max}$. The parameter J_{eff} was obtained by fitting the magnetic susceptibility data as described in the Supplementary Information, using an equation based on an isotropic Heisenberg Hamiltonian (Supplementary Fig. S12). If we assume that the coupling constant, J_0, describing the Heisenberg exchange interaction, did not change compared to **14** ($J_0 = -6$ cm^{-1}), then the extracted values $\omega = 3{,}341$ cm^{-1} and $J_{eff} = 23$ cm^{-1} can be used to obtain $B = 220$ cm^{-1}. This value likely provides a more realistic estimate compared with the aforementioned B values obtained from the fully delocalized model. Clearly, a more detailed theoretical understanding of the electronic structure of molecules such as $[(PY5Me_2)_2V_2(\mu\text{-}5,6\text{-dmbzim})]^{4+}$ is essential for the accurate analysis of experimental results for mixed-valence coordination clusters featuring double exchange.

Outlook

The foregoing results demonstrate that simple organic bridging ligands such as imidazolate can be used to generate molecules possessing well-isolated high-spin ground states through a double-exchange mechanism, as exemplified here with dinuclear complexes of the type $[(PY5Me_2)V(\mu\text{-}L_{br})V(PY5Me_2)]^{4+}$. Significantly, imidazolate and derivatives thereof have already been shown to serve as bridging ligands in a variety of larger coordination clusters[47,48], as well as a broad series of microporous metal–organic frameworks[49,50]. Thus, there are good prospects for the possible generation of electron-delocalized coordination clusters with significantly higher spin ground states and metal–organic frameworks that behave as microporous magnets. Along these lines, efforts are currently under way to generate imidazolate-bridged squares of the type $[(L_{cap})_4V_4(\mu\text{-}L_{br})_4]^{5+}$ (with a predicted $S = 11/2$ ground state), cubes of the type $[(L_{cap})_8V_8(\mu\text{-}L_{br})_{12}]^{5+}$ (with a predicted $S = 23/2$ ground state) and magnetic solids of the type $A_x^I[V(\mu\text{-}L_{br})_3]$. In addition, we will attempt to enhance the degree of electron delocalization in such species through replacement of the vanadium centres with early second- and third-row transition metals, which could perhaps lead to clusters exhibiting high-spin ground states that persist at room temperature. Ultimately, such species might even find applications as single-molecule magnets or MRI contrast agents.

References

1. Sessoli, R., Gatteschi, D., Caneschi, A. & Novak, M. A. Magnetic bistability in a metal-ion cluster. *Nature* **365,** 141–143 (1993).
2. Barra, A.-L., Debrunner, P., Gatteschi, D. Schulz, C. E. & Sessoli, R. Superparamagnetic-like behavior in an octanuclear iron cluster. *Europhys. Lett.* **35,** 133–138 (1996).
3. Gatteschi, D., Sessoli, R. & Villain, J. *Molecular Nanomagnets* (Oxford Univ. Press, 2006).
4. Milios, C. J. *et al.* A record anisotropy barrier for a single-molecule magnet. *J. Am. Chem. Soc.* **129,** 2754–2755 (2007).
5. Garanin, D. A. & Chudnovsky, E. M. Thermally activated resonant magnetization tunneling in molecular magnets: Mn$_{12}$Ac and others. *Phys. Rev. B* **56,** 11102–11118 (1997).
6. Leuenberger, M. N. & Loss, D. Quantum computing in molecular systems. *Nature* **410,** 789–793 (2001).

7. Heersche, H. B. *et al*. Electron transport through single Mn$_{12}$ molecular magnets. *Phys. Rev. Lett.* **96,** 206801 (2006).
8. Kübler, J. *Theory of Itinerant Electron Magnetism* (Oxford Univ. Press, 2000).
9. Liu, Y., Sellmyer, D. J. & Shindo, D. eds. *Handbook of Advanced Magnetic Materials, Volume 4: Properties and Applications* (Springer, 2006).
10. Caulder, D. L. & Raymond, K. N. The rational design of high symmetry coordination clusters. *J. Chem. Soc. Dalton Trans.* 1185–1200 (1999).
11. Ruben, M., Rojo, J., Romero-Salguero, F. J., Uppadine, L. H. & Lehn, J.-M. Grid-type metal ion architectures: functional metallosupramolecular arrays. *Angew. Chem. Int. Ed.* **43,** 3644–3662 (2004).
12. Fujita, M., Tominaga, M., Hori, A. & Therrien, B. Coordination assemblies from a Pd(II)-cornered square complex. *Acc. Chem. Res.* **38,** 371–380 (2005).
13. Beltran, L. M. C. & Long, J. R. Directed assembly of metal–cyanide cluster magnets. *Acc. Chem. Res.* **38,** 325–334 (2005).
14. Ako, A. M. *et al*. A ferromagnetically coupled Mn$_{19}$ aggregate with a record $S = 83/2$ ground spin state. *Angew. Chem. Int. Ed.* **45,** 4926–4929 (2006).
15. Creutz, C. & Taube, H. Binuclear complexes of ruthenium ammines. *J. Am. Chem. Soc.* **95,** 1086–1094 (1973).
16. Hush, N. S. Intervalence-transfer absorption. Part 2. Theoretical considerations and spectroscopic data. *Prog. Inorg. Chem.* **8,** 391–444 (1967).
17. Mayoh, B. & Day, P. Charge transfer in mixed-valence solids. Part VIII. Contribution of valence delocalization to the ferromagnetism of Prussian blue. *J. Chem. Soc. Dalton Trans.* 1483–1486 (1976).
18. Creutz, C. Mixed valence complexes of d^5–d^6 metal centers. *Prog. Inorg. Chem.* **30,** 1–73 (1983).
19. Demadis, K. D., Hartshorn, C. M. & Meyer, T. J. The localised-to-delocalised transition in mixed-valence chemistry. *Chem. Rev.* **101,** 2655–2685 (2001).
20. Brunschwig, B. S., Creutz, C. & Sutin, N. Optical transitions of symmetrical mixed-valence systems in the class II–III transition regime. *Chem. Soc. Rev.* **31,** 168–184 (2002).
21. D'Alessandro, D. M. & Keene. F. R. Current trends and future challenges in the experimental, theoretical and computational analysis of intervalence charge transfer (IVCT) transitions. *Chem. Soc. Rev.* **35,** 424–440 (2006).
22. Robin, M. B. & Day. P. Mixed-valence chemistry—a survey and classification. *Adv. Inorg. Chem. Radiochem.* **10,** 247–403 (1967).
23. Zener, C. Interaction between the *d*-shells in the transition metals. II. Ferromagnetic compounds of manganese with perovskite structure. *Phys. Rev.* **82,** 403–405 (1951).
24. Baerner, K. & Yang, C. P. *Double Exchange in Heusler Alloys and Related Materials* (Research Signpost, 2007).
25. Girerd, J.-J. Electron transfer between magnetic ions in mixed valence binuclear systems. *J. Chem. Phys.* **79,** 1766–1775 (1983).
26. Drillon, M., Pourroy, G. & Darriet, J. Electronic and vibronic coupling in a mixed-valence dimeric unit d^1–d^2, magnetic aspects. *Chem. Phys.* **88,** 27–37 (1984).
27. Noodleman, L. & Baerends, E. J. Electronic structure, magnetic properties, ESR and optical spectra for 2-iron ferredoxin models by LCAO-Xα valence bond theory. *J. Am. Chem. Soc.* **106,** 2316–2327 (1984).
28. Blondin, G. & Girerd, J.-J. Interplay of electron exchange and electron transfer in metal polynuclear complexes in proteins or chemical models. *Chem. Rev.* **90,** 1359–1376 (1990).
29. Borras-Almenar, J. J., Coronado, E., Ostrovsky, S. M., Palii, A. V. & Tsukerblat, B. S. Localization vs. delocalization in the dimeric mixed-valence clusters in the generalized vibronic model. Magnetic manifestations. *Chem. Phys.* **240,** 149–161 (1999).
30. Yang, X., Hu, H. & Chen, Z. Effect of magnetic exchange, double exchange, vibronic coupling and asymmetry on magnetic properties in d^2–d^3 mixed-valence dimers. *Int. J. Quant. Chem.* **103,** 190–197 (2005).
31. Beissel, T. *et al*. Exchange and double-exchange phenomena in linear homo- and heterotrinuclear nickel(II,III,IV) complexes containing six μ$_2$-phenolato or μ$_2$-thiophenolato bridging ligands. *J. Am. Chem. Soc.* **118,** 12376–12390 (1996).
32. Saal, C. *et al*. Magnetic investigations on a valence-delocalized Fe(II)–Fe(III) complex. *Ber. Bunsenges. Phys. Chem.* **100,** 2086–2090 (1996).
33. Shores, M. P. & Long, J. R. Tetracyanide-bridged divanadium complexes: redox switching between strong antiferromagnetic and strong ferromagnetic coupling. *J. Am. Chem. Soc.* **124,** 3512–3513 (2002).
34. Drüeke, S. *et al*. The novel mixed-valence, exchange-coupled, class III dimer [L$_2$Fe$_2$(μ-OH)$_3$]$^{2+}$ (L=*N,N′,N′′*-trimethyl-1,4,7-triazacyclononane). *Chem. Commun.* **1,** 59–62 (1989).
35. Ding, X.-Q. *et al*. Mössbauer and electron paramagnetic resonance study of the double-exchange and Heisenberg-exchange interactions in a novel binuclear iron(II/III) delocalized-valence compound. *J. Chem. Phys.* **92,** 178–186 (1990).
36. Gamelin, D. R., Bominaar, E. L., Kirk, M. L., Wieghardt, K. & Solomon, E. I. Excited-state contributions to ground-state properties of mixed-valence dimers: spectral and electronic-structural studies of [Fe$_2$(OH)$_3$(tmtacn)$_2$]$^{2+}$ related to the [Fe$_2$S$_2$]$^+$ active sites of plant-type ferredoxins. *J. Am. Chem. Soc.* **118,** 8085–8097 (1996).
37. Barone, V., Bencini, A., Ciofini, I., Daul, C. A. & Totti, F. Density functional modeling of double exchange interactions in transition metal complexes. Calculation of the ground and excited state properties of [Fe$_2$(OH)$_3$(tmtacn)$_2$]$^{2+}$. *J. Am. Chem. Soc.* **120,** 8357–8365 (1998).
38. Dyker, G. & Muth, O. Synthesis of methylene- and methine-bridged oligopyridines. *Eur. J. Org. Chem.* **21,** 4319–4322 (2004).
39. Goldsmith, C. R., Jonas, R. T., Cole, A. P. & Stack, T. D. P. A spectrochemical walk: single-site perturbation within a series of six-coordinate ferrous complexes. *Inorg. Chem.* **41,** 4642–4652 (2002).
40. Gebbink, R. J. M. K., Jonas, R. T., Goldsmith, C. R. & Stack, T. D. P. A periodic walk: a series of first-row transition metal complexes with the pentadentate ligand PY5. *Inorg. Chem.* **41,** 4633–4641 (2002).
41. Canty, A. J., Minchin, N. J., Skelton, B. W. & White, A. H. Interaction of palladium(II) acetate with substituted pyridines, including a cyclometallation reaction and the structure of (acetato-*O*){meso-2,6-*bis*[1-phenyl-1-(pyridin-2-yl)ethyl]pyridine-*N,N′,N′′*}palladium(II) acetate trihydrate. *J. Chem. Soc. Dalton Trans.* 2205–2210 (1986).
42. LeSuer, R. & Geiger, W. E. Improved electrochemistry in low-polarity media using tetrakis(pentafluorophenyl)borate salts as supporting electrolytes. *Angew. Chem. Int. Ed.* **39,** 248–250 (2000).
43. Zavarine, I. S. & Kubiak, C. P. A versatile variable temperature thin layer reflectance spectroelectrochemical cell. *J. Electroanal. Chem.* **495,** 106–109 (2001).
44. Ciampolini, M. & Mani, F. Vanadium(II) complexes of substituted imidazoles. *Inorg. Chim. Acta* **24,** 91–95 (1977).
45. Larkworthy, L. F. & Tucker, B. J. Hexaisothiocyanates of vanadium(II). *J. Chem. Soc. Dalton Trans.* 2042–2043 (1980).
46. Miller, J. S. & Drillon, M. *Magnetism: Molecules to Materials* 155 (Wiley-VCH, 2001).
47. Liu, Y., Kravtsov, V., Walsh, R. D., Poddar, P., Srikanth, H. & Eddaoudi, M. Directed assembly of metal–organic cubes from deliberately predesigned molecular building blocks. *Chem. Commun.* 2806–2807 (2004).
48. Dinca, M., Harris, T. D., Iavarone, A. T. & Long, J. R. Synthesis and characterization of the cubic coordination cluster [Co$_6^{III}$Co$_2^{II}$(IBT)$_{12}$]$^{14-}$ (H$_3$IBT=4,5-*bis*(tetrazol-5-yl)imidazole). *J. Mol. Struct.* **890,** 139–143 (2008).
49. Liu, Y., Kravtsov, V. C., Larsen, R. & Eddaoudi, M. Molecular building blocks approach to the assembly of zeolite-like metal–organic frameworks (ZMOFs) with extra-large cavities. *Chem. Commun.* 1488–1490 (2006).
50. Park, K. S. *et al*. Exceptional chemical and thermal stability of zeolitic imidazolate frameworks. *Proc. Natl Acad. Sci. USA* **103,** 10186–10191 (2006).

Author contributions
B.B., D.M.D. and D.M.J. performed the majority of the experiments and data analysis. A.T.I. collected and analysed the mass spectrometry data. S.D.G. and C.P.K. assisted with acquisition of the FT-IR spectroelectrochemical data. J.R.L. designed and supervised the research. The paper was written by B.B., D.M.D. and J.R.L., and all authors discussed the results and commented on the manuscript.

Additional information
The authors declare no competing financial interests. Supplementary information and chemical compound information accompany this paper at www.nature.com/naturechemistry. Reprints and permission information is available online at http://npg.nature.com/reprintsandpermissions/. Correspondence and requests for materials should be addressed to J.R.L.